NASA TECHNICAL NOTE

NASA TN D-4265

NASA TN D-4265

NONLINEAR FLUTTER OF
A CIRCULAR CYLINDRICAL SHELL
IN SUPERSONIC FLOW

by

David A. Evensen

Langley Research Center
Langley Station, Hampton, Va.

and

Mervyn D. Olson

National Aeronautical Establishment
Ottawa, Canada

NONLINEAR FLUTTER OF A CIRCULAR CYLINDRICAL SHELL

IN SUPERSONIC FLOW

By David A. Evensen

Langley Research Center
Langley Station, Hampton, Va.

and

Mervyn D. Olson

National Aeronautical Establishment
Ottawa, Canada

NATIONAL AERONAUTICS AND SPACE ADMINISTRATION

NONLINEAR FLUTTER OF A CIRCULAR CYLINDRICAL SHELL

IN SUPERSONIC FLOW[*]

By David A. Evensen
NASA Langley Research Center, Hampton, Virginia

and Mervyn D. Olson
National Aeronautical Establishment, Ottawa, Canada

SUMMARY

A nonlinear analysis is presented for calculating the limiting amplitudes of cylin-drical shell flutter by using a four-mode approximation for the shell deflection. The aerodynamic pressure is approximated by linear piston theory, and the nonlinearity enters the problem through the nonlinear shallow-shell equations for the cylinder. The governing equations are reduced to four modal equations by applying Galerkin's method, and limit cycle solutions are obtained by the method of harmonic balance. Stability of the limit cycles is investigated numerically by integrating the modal equations on a digital computer.

Two types of limit cycle flutter are obtained: (a) two-mode standing-wave flutter and (b) four-mode circumferentially traveling-wave flutter. Under most conditions, the two-mode standing-wave flutter becomes unstable and transforms into four-mode traveling-wave flutter. The analysis indicates that flutter can occur at aerodynamic pressures below the linear flutter boundary. This fact may explain why recent results indicate a difference between experiments and linear theory for the flutter of cylindrical shells.

INTRODUCTION

The self-excited oscillation of thin plates exposed on one side to a parallel super-sonic airstream is called panel flutter. For some aerospace applications, the prevention of this flutter instability becomes the primary design criterion for the structure.

Although panel flutter is usually associated with flat or curved plates, a thin-walled cylindrical shell can also exhibit this type of instability. Extensive reviews of the panel

flutter problem and analyses dealing with the flutter of cylindrical shells are given in references 1 to 3. Experimental observations of cylindrical shell flutter are reported in references 4 and 5.

A striking feature of the results of reference 5 is the fact that "almost all the flutter modes observed in these experiments were of the circumferentially traveling-wave type." Such traveling waves are not predicted by linear theory, and it was suggested in reference 5 that nonlinearities in the shell were responsible for the phenomenon. This suggestion motivated the present study, the purpose of which is to demonstrate that the circumferentially traveling-wave flutter can be predicted from a nonlinear analysis.

Some introductory work on the nonlinear flutter of cylindrical shells appears in reference 6, which employed a two-mode approximation to the shell deflection. The present study utilizes four modes, the minimum number required to yield traveling-wave flutter. In addition, the present analysis retains higher order nonlinear terms which were neglected in reference 6. Thus, the present study extends the results of previous work to include the possibility of traveling-wave flutter and to examine the influence of higher order nonlinearities.

The aerodynamic pressure acting on the shell is approximated by linear piston theory, which is commonly used for the high Mach numbers of interest in this study. At the present time, no completely acceptable aerodynamic theory is available for cylindrical shell flutter. However, in reference 6 it is shown that flutter predictions based on piston theory correspond fairly close to experimental findings, at least for moderate amounts of internal pressure in the shell. Furthermore, piston theory is by far the simplest theory to apply to flutter calculations. Note that there is no real contradiction in using linear aerodynamic theory for nonlinear flutter calculations, because the limiting amplitudes of flutter will still be within the linear range from the aerodynamic point of view.

The cylindrical shell is represented by the nonlinear shallow-shell equations, and a Galerkin procedure is used to reduce the problem to four coupled ordinary nonlinear differential equations for the modal amplitudes. Approximate limit cycle solutions to these modal equations are obtained by the method of harmonic balance. These approximate limit cycles were verified and their stability was investigated by numerically integrating the modal equations on a digital computer.

The limit cycle solutions for flutter fall into two categories. The first type of flutter involves only two modes, whereas the second type involves four modes responding together in a very special way. The two-mode flutter is similar to the standing-wave flutter investigated in reference 6 (and, in fact, is very similar to the flutter of flat panels), whereas the four-mode flutter involves circumferentially traveling waves. This latter phenomenon is characteristic of axisymmetric structures. A noteworthy feature of

2

the four-mode limit cycle results in the conclusion that flutter can occur below the boundary predicted by linear theory. This observation might explain why cylindrical shell flutter has been found experimentally to occur below the theoretical linear flutter boundary.

SYMBOLS

a_∞ free-stream speed of sound

$\left.\begin{array}{l} A_1(t), A_2(t) \\ B_1(t), B_2(t) \end{array}\right\}$ generalized coordinates of assumed modes

$\left.\begin{array}{l} a_1(t), a_2(t) \\ b_1(t), b_2(t) \end{array}\right\}$ nondimensional generalized coordinates; $a_1 = A_1/h, \ldots$

A, B, C, D limit cycle amplitudes (see eq. (8))

D_s shell bending stiffness, $Eh^3/12(1 - \nu^2)$

E Young's modulus

F stress function, defined by $\begin{cases} N_x = \dfrac{1}{R^2} \dfrac{\partial^2 F}{\partial \theta^2} \\[2ex] N_{x\theta} = -\dfrac{1}{R} \dfrac{\partial^2 F}{\partial x\, \partial \theta} \\[2ex] N_\theta = \dfrac{\partial^2 F}{\partial x^2} \end{cases}$

f, f_0 aerodynamic pressure parameters (eq. (6))

h thickness of shell wall

i, j integers, ranging from 1 to 4

$K_j(x_i)$ functional notation to denote equations (11) or (15)

$\left.\begin{array}{l} k_1 \ldots k_5 \\ \ell_1 \ldots \ell_6 \end{array}\right\}$ coefficients defined in appendix A

3

L	length of cylindrical shell
M_∞	free-stream Mach number of airstream
m,n	axial and circumferential wave numbers
$\overline{N}_x, \overline{N}_\theta$	stress resultants due to applied loads
p	pressure
p_∞	free-stream static pressure
p_m	shell internal pressure (net)
R	radius of cylindrical shell
t	time
u,v,w	median surface displacements of shell (fig. 1)
x, θ, z	coordinates in the axial, circumferential, and radial directions, respectively (see fig. 1)
x_l	vector representation of the unknowns B, ω, f, and ϕ (see eqs. (C2))
x_{io}	initial approximation to solution of equations (C2)
γ	gas constant, 1.4
δ_{x_i}	corrections to vector x_{io}
Δ, Δ', ζ	damping parameters (see eq. (12))
ϵ	nonlinearity parameter (eq. (7))
$\kappa = 3L/8M_\infty a_\infty$	
ν	Poisson's ratio

4

ρ_s shell material density

σ aspect ratio of shell displacement, $\pi R/nL$

ϕ, ψ, χ steady-state phase angles

ω, ω_0 flutter or vibration frequencies

ω_{1n}, ω_{2n} linear undamped modal frequencies (appendix B)

A dot over a quantity indicates differentiation with respect to time.

THEORY

In the following sections, the governing equations for a cylindrical shell are presented and briefly discussed. A four-mode solution is assumed, and Galerkin's method is applied to reduce the problem to one involving ordinary differential equations. Approximate limit cycle solutions to these equations are obtained by the method of harmonic balance. Stability of the limit cycle flutter is also discussed.

Governing Equations

The nonlinear shallow-shell equations form the starting point for this investigation. These equations make use of Donnell's approximations for cylindrical shells and are derived in reference 7. In terms of the radial deflection w and in a common notation, these equations are

$$D_S \nabla^4 w + \rho_s h \frac{\partial^2 w}{\partial t^2} + p = \overline{N}_x \frac{\partial^2 w}{\partial x^2} + \frac{\overline{N}_\theta}{R^2} \frac{\partial^2 w}{\partial \theta^2} + \frac{1}{R} \frac{\partial^2 F}{\partial x^2} + \frac{1}{R^2} \left(\frac{\partial^2 F}{\partial \theta^2} \frac{\partial^2 w}{\partial x^2} - 2 \frac{\partial^2 F}{\partial x \, \partial \theta} \frac{\partial^2 w}{\partial x \, \partial \theta} + \frac{\partial^2 F}{\partial x^2} \frac{\partial^2 w}{\partial \theta^2} \right)$$

(1)

and

$$\frac{1}{Eh} \nabla^4 F = -\frac{1}{R} \frac{\partial^2 w}{\partial x^2} + \frac{1}{R^2} \left[\left(\frac{\partial^2 w}{\partial x \, \partial \theta} \right)^2 - \frac{\partial^2 w}{\partial x^2} \frac{\partial^2 w}{\partial \theta^2} \right]$$

(2)

where w is the radial deflection of the shell and F is the usual stress function. The shell geometry and coordinate system are shown in figure 1.

The aerodynamic pressure p is approximated by first-order piston theory, which yields
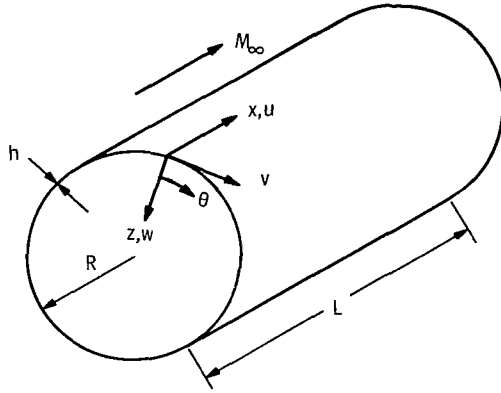
$$p = \gamma p_\infty \left(\frac{1}{a_\infty} \frac{\partial w}{\partial t} + M_\infty \frac{\partial w}{\partial x} \right) \qquad (3)$$

In writing equations (1) to (3), the reader will note that (1) in-plane inertia terms have been neglected, and (2) the equations are written for w defined positive inward (fig. 1) and p defined positive outward.

Figure 1.- Shell geometry and coordinate system.

Four-Mode Approximation — Galerkin's Method

Equations (1) to (3) are solved approximately by using a four-mode deflection of the form:

$$w(x,\theta,t) = \left[A_1(t)\sin\frac{\pi x}{L} + A_2(t)\sin\frac{2\pi x}{L} \right]\cos n\theta + \left[B_1(t)\sin\frac{\pi x}{L} + B_2(t)\sin\frac{2\pi x}{L} \right]\sin n\theta$$

$$+ \frac{n^2}{4R}\left[A_1(t)\sin\frac{\pi x}{L} + A_2(t)\sin\frac{2\pi x}{L} \right]^2 + \frac{n^2}{4R}\left[B_1(t)\sin\frac{\pi x}{L} + B_2(t)\sin\frac{2\pi x}{L} \right]^2 \qquad (4)$$

These mode shapes are similar to those used previously by the author in the nonlinear vibrations of cylindrical shells (ref. 8) and verified experimentally for the nonlinear vibrations of rings (ref. 9). The terms which are multiplied by $n^2/4R$ are included in equation (4) so that the solution will satisfy the periodic continuity condition on the circumferential displacement v.

Substitution of equation (4) into the compatibility equation (2) allows the latter to be solved for a particular solution F, which is given in appendix A. The complementary solution to equation (2) is taken to be zero. By substituting w and F into the appropriate nonlinear strain-displacement relations of shallow-shell theory, it can be shown that the following conditions are satisfied:

(a) The displacements u, v, and w and their derivatives satisfy periodic continuity conditions of the form:

$$v(x,\theta,t) = v(x,\theta + 2\pi,t)$$

(b) The deflection w goes to zero at the ends of the shell, that is, at x = 0 and x = L.

(c) The boundary conditions for a shell having freely supported ends are satisfied to a first approximation. For example, the axial bending moment is composed of terms which involve the amplitudes A_1 and B_1 linearly and nonlinear terms involving

products of A_1, B_1, and so forth. At the ends of the shell, the linear terms go to zero, but the nonlinear terms do not vanish. A similar situation is true for N_x and v, where the nonlinear terms do not go to zero at the ends of the shell. Since the nonlinear terms are relatively small, it is felt that these boundary conditions approximate those of a freely supported shell.

Finally, the expressions for w, F, and p are substituted into equation (1), and a Galerkin procedure is used to obtain four coupled nonlinear ordinary differential equations for the modal amplitudes A_1 to B_2. The expressions $\partial w/\partial A_1$, $\partial w/\partial A_2$, $\partial w/\partial B_1$, and $\partial w/\partial B_2$ were used as the weighting functions in the Galerkin procedure. In a partly nondimensionalized form, the resulting coupled equations are

$$\ddot{a}_1 + \Delta\dot{a}_1 + \omega_{1n}{}^2 a_1 - fa_2 + \frac{3\epsilon}{8} a_1\left(a_1\ddot{a}_1 + \dot{a}_1{}^2 + b_1\ddot{b}_1 + \dot{b}_1{}^2\right) + \frac{\epsilon a_1}{4}\left(a_2\ddot{a}_2 + \dot{a}_2{}^2 + b_2\ddot{b}_2 + \dot{b}_2{}^2\right)$$

$$+ \frac{\epsilon a_2}{4}\left(a_1\ddot{a}_2 + 2\dot{a}_1\dot{a}_2 + a_2\ddot{a}_1 + b_1\ddot{b}_2 + 2\dot{b}_1\dot{b}_2 + b_2\ddot{b}_1\right) + \frac{\epsilon\Delta}{8}\left[3a_1\left(a_1\dot{a}_1 + b_1\dot{b}_1\right) + 2a_1\left(a_2\dot{a}_2 + b_2\dot{b}_2\right)\right.$$

$$\left. + 2a_2\left(a_2\dot{a}_1 + a_1\dot{a}_2 + b_2\dot{b}_1 + b_1\dot{b}_2\right)\right] - \frac{\epsilon f}{5}\left[2a_1\left(a_1a_2 + b_1b_2\right) - a_2\left(a_1{}^2 + b_1{}^2\right) + \frac{4}{7}a_2\left(a_2{}^2 + b_2{}^2\right)\right]$$

$$- \epsilon k_1 a_1\left(a_1{}^2 + b_1{}^2\right) + \epsilon k_2\left[a_1\left(a_1{}^2 - b_1{}^2\right) + 4a_1\left(a_2{}^2 - b_2{}^2\right) + 2b_1\left(a_1b_1 + 4a_2b_2\right)\right]$$

$$- \epsilon k_3 a_2\left(a_1a_2 + b_1b_2\right) + \epsilon k_4 a_1\left(a_2{}^2 + b_2{}^2\right) + \epsilon^2 l_1 a_1\left(a_1{}^2 + b_1{}^2\right)^2 + \epsilon^2 l_2\left[a_2\left(a_1{}^2 + b_1{}^2\right)\right.$$

$$\left. \times \left(a_1a_2 + b_1b_2\right) + a_1\left(a_1a_2 + b_1b_2\right)^2\right] + \epsilon^2 l_3 a_2\left(a_2{}^2 + b_2{}^2\right)\left(a_1a_2 + b_1b_2\right)$$

$$- 2\epsilon^2 l_4 a_1\left(a_1{}^2 + b_1{}^2\right)\left(a_2{}^2 + b_2{}^2\right) + \epsilon^2 l_5 a_1\left(a_2{}^2 + b_2{}^2\right)^2 = 0 \qquad (5a)$$

$$\ddot{a}_2 + \Delta\dot{a}_2 + \omega_{2n}{}^2 a_2 + fa_1 + \frac{3\epsilon}{8} a_2\left(a_2\ddot{a}_2 + \dot{a}_2{}^2 + b_2\ddot{b}_2 + \dot{b}_2{}^2\right) + \frac{\epsilon a_2}{4}\left(a_1\ddot{a}_1 + \dot{a}_1{}^2 + b_1\ddot{b}_1 + \dot{b}_1{}^2\right)$$

$$+ \frac{\epsilon a_1}{4}\left(a_1\ddot{a}_2 + 2\dot{a}_1\dot{a}_2 + a_2\ddot{a}_1 + b_1\ddot{b}_2 + 2\dot{b}_1\dot{b}_2 + b_2\ddot{b}_1\right) + \frac{\epsilon\Delta}{8}\left[3a_2\left(a_2\dot{a}_2 + b_2\dot{b}_2\right) + 2a_2\left(a_1\dot{a}_1 + b_1\dot{b}_1\right)\right.$$

$$\left. + 2a_1\left(a_1\dot{a}_2 + a_2\dot{a}_1 + b_1\dot{b}_2 + b_2\dot{b}_1\right)\right] + \frac{\epsilon f}{5}\left[a_1\left(a_1{}^2 + b_1{}^2\right) + \frac{8}{7}a_2\left(a_1a_2 + b_1b_2\right) - \frac{4}{7}a_1\left(a_2{}^2 + b_2{}^2\right)\right]$$

$$+ 4\epsilon k_2\left[4a_2\left(a_2{}^2 - b_2{}^2\right) + a_2\left(a_1{}^2 - b_1{}^2\right) + 2b_2\left(a_1b_1 + 4a_2b_2\right)\right] - \epsilon k_3 a_1\left(a_1a_2 + b_1b_2\right)$$

$$+ \epsilon k_4 a_2\left(a_1{}^2 + b_1{}^2\right) - \epsilon k_5 a_2\left(a_2{}^2 + b_2{}^2\right) + \epsilon^2 l_2 a_1\left(a_1{}^2 + b_1{}^2\right)\left(a_1 a_2 + b_1 b_2\right) + \epsilon^2 l_3\Big[a_1\left(a_2{}^2 + b_2{}^2\right)$$

$$\times \left(a_1 a_2 + b_1 b_2\right) + a_2\left(a_1 a_2 + b_1 b_2\right)^2\Big] - \epsilon^2 l_4 a_2\left(a_1{}^2 + b_1{}^2\right)^2 + 2\epsilon^2 l_5 a_2\left(a_1{}^2 + b_1{}^2\right)\left(a_2{}^2 + b_2{}^2\right)$$

$$+ \epsilon^2 l_6 a_2\left(a_2{}^2 + b_2{}^2\right)^2 = 0 \tag{5b}$$

$$\ddot{b}_1 + \Delta \dot{b}_1 + \omega_{1n}{}^2 b_1 - f b_2 + \frac{3\epsilon}{8} b_1\left(a_1\ddot{a}_1 + \dot{a}_1{}^2 + b_1\ddot{b}_1 + \dot{b}_1{}^2\right) + \frac{\epsilon b_1}{4}\left(a_2\ddot{a}_2 + \dot{a}_2{}^2 + b_2\ddot{b}_2 + \dot{b}_2{}^2\right)$$

$$+ \frac{\epsilon b_2}{4}\left(a_1\ddot{a}_2 + 2\dot{a}_1\dot{a}_2 + a_2\ddot{a}_1 + b_1\ddot{b}_2 + 2\dot{b}_1\dot{b}_2 + b_2\ddot{b}_1\right) + \frac{\epsilon \Delta}{8}\Big[3 b_1\left(a_1\dot{a}_1 + b_1\dot{b}_1\right) + 2 b_1\left(a_2\dot{a}_2 + b_2\dot{b}_2\right)$$

$$+ 2 b_2\left(a_1\dot{a}_2 + a_2\dot{a}_1 + b_1\dot{b}_2 + b_2\dot{b}_1\right)\Big] - \frac{\epsilon f}{5}\Big[2 b_1\left(a_1 a_2 + b_1 b_2\right) - b_2\left(a_1{}^2 + b_1{}^2\right) + \frac{4}{7} b_2\left(a_2{}^2 + b_2{}^2\right)\Big]$$

$$- \epsilon k_1 b_1\left(a_1{}^2 + b_1{}^2\right) + \epsilon k_2\Big[b_1\left(b_1{}^2 - a_1{}^2\right) + 4 b_1\left(b_2{}^2 - a_2{}^2\right) + 2 a_1\left(a_1 b_1 + 4 a_2 b_2\right)\Big]$$

$$- \epsilon k_3 b_2\left(a_1 a_2 + b_1 b_2\right) + \epsilon k_4 b_1\left(a_2{}^2 + b_2{}^2\right) + \epsilon^2 l_1 b_1\left(a_1{}^2 + b_1{}^2\right)^2 + \epsilon^2 l_2\Big[b_2\left(a_1{}^2 + b_1{}^2\right)$$

$$\times \left(a_1 a_2 + b_1 b_2\right) + b_1\left(a_1 a_2 + b_1 b_2\right)^2\Big] + \epsilon^2 l_3 b_2\left(a_2{}^2 + b_2{}^2\right)\left(a_1 a_2 + b_1 b_2\right) - 2\epsilon^2 l_4 b_1\left(a_1{}^2 + b_1{}^2\right)$$

$$\times \left(a_2{}^2 + b_2{}^2\right) + \epsilon^2 l_5 b_1\left(a_2{}^2 + b_2{}^2\right)^2 = 0 \tag{5c}$$

$$\ddot{b}_2 + \Delta \dot{b}_2 + \omega_{2n}{}^2 b_2 + f b_1 + \frac{3\epsilon}{8} b_2\left(a_2\ddot{a}_2 + \dot{a}_2{}^2 + b_2\ddot{b}_2 + \dot{b}_2{}^2\right) + \frac{\epsilon b_2}{4}\left(a_1\ddot{a}_1 + \dot{a}_1{}^2 + b_1\ddot{b}_1 + \dot{b}_1{}^2\right)$$

$$+ \frac{\epsilon b_1}{4}\left(a_1\ddot{a}_2 + 2\dot{a}_1\dot{a}_2 + a_2\ddot{a}_1 + b_1\ddot{b}_2 + 2\dot{b}_1\dot{b}_2 + b_2\ddot{b}_1\right) + \frac{\epsilon \Delta}{8}\Big[3 b_2\left(a_2\dot{a}_2 + b_2\dot{b}_2\right) + 2 b_2\left(a_1\dot{a}_1 + b_1\dot{b}_1\right)$$

$$+ 2 b_1\left(a_1\dot{a}_2 + a_2\dot{a}_1 + b_1\dot{b}_2 + b_2\dot{b}_1\right)\Big] + \frac{\epsilon f}{5}\Big[b_1\left(a_1{}^2 + b_1{}^2\right) - \frac{4}{7} b_1\left(a_2{}^2 + b_2{}^2\right) + \frac{8}{7} b_2\left(a_1 a_2 + b_1 b_2\right)\Big]$$

$$+ 4\epsilon k_2\Big[4 b_2\left(b_2{}^2 - a_2{}^2\right) + b_2\left(b_1{}^2 - a_1{}^2\right) + 2 a_2\left(a_1 b_1 + 4 a_2 b_2\right)\Big] - \epsilon k_3 b_1\left(a_1 a_2 + b_1 b_2\right)$$

$$+ \epsilon k_4 b_2\left(a_1{}^2 + b_1{}^2\right) - \epsilon k_5 b_2\left(a_2{}^2 + b_2{}^2\right) + \epsilon^2 l_2 b_1\left(a_1{}^2 + b_1{}^2\right)\left(a_1 a_2 + b_1 b_2\right) + \epsilon^2 l_3$$

$$\left[b_1\left(a_2{}^2 + b_2{}^2\right)\left(a_1a_2 + b_1b_2\right) + b_2\left(a_1a_2 + b_1b_2\right)^2 \right] - \epsilon^2 l_4 b_2\left(a_1{}^2 + b_1{}^2\right)^2 + 2\epsilon^2 l_5 b_2\left(a_1{}^2 + b_1{}^2\right)$$

$$\times \left(a_2{}^2 + b_2{}^2\right) + \epsilon^2 l_6 b_2\left(a_2{}^2 + b_2{}^2\right)^2 = 0 \tag{5d}$$

where a_1, a_2, b_1, and b_2 are the nondimensional modal amplitudes. The linear modal frequencies are designated by ω_{1n} and ω_{2n} (see appendix B), and the aerodynamic influence comes through the two parameters

$$\left. \begin{array}{l} \Delta = \dfrac{\gamma p_\infty}{\rho_s h a_\infty} \\[2em] f = \dfrac{8\gamma M_\infty p_\infty}{3\rho_s Lh} \end{array} \right\} \tag{6}$$

The nonlinearity parameter ϵ is given by

$$\epsilon = \left(\frac{n^2 h}{R}\right)^2 \tag{7}$$

Note that the equations become linear when $\epsilon = 0$. The coefficients k_1 to k_5 and l_1 to l_6 in equations (5) depend upon the shell material properties, mode shapes, and the axial membrane stress resultant $\overline{N}_x$; they are defined in appendix B.

Limit Cycle Oscillations — Method of Harmonic Balance

According to linear flutter theory, disturbances of the modal amplitudes away from zero are damped with time as long as the aerodynamic pressure parameter f is below the linear flutter boundary, given by $f = f_0$. Conversely, when f is greater than f_0, the linear theory predicts that disturbances of the modal amplitudes will increase exponentially with time. However, when nonlinear terms are included in the analysis, the situation is altered considerably. The nonlinear terms restrict the growth in amplitude, and eventually a steady-state vibration with finite amplitude is usually obtained. Such a vibration is termed a "limit cycle oscillation." (See ref. 10 for a discussion of limit cycles in nonlinear self-excited systems.)

Equations (5) exhibit limit cycle oscillations of the type just described. When the nonlinearities are relatively small (for example, $\epsilon k_i \ll \omega_{1n}{}^2$), the limit cycle vibrations are nearly sinusoidal in time. In this case, the method of "harmonic balance" (ref. 11) can be used to obtain approximate solutions for the limiting amplitudes and phases.

To obtain approximate limit cycle solutions to equations (5), the amplitudes $a_1(t)$ to $b_2(t)$ are assumed to be in the general form:

9

$$a_1(t) = A \cos \omega t$$
$$a_2(t) = B \cos(\omega t + \phi)$$
$$b_1(t) = C \cos(\omega t + \psi)$$
$$b_2(t) = D \cos(\omega t + \chi)$$

(8)

that is, the limit cycle vibrations are assumed to be sinusoidal in time. To apply the method of harmonic balance, equations (8) are substituted first into equation (5a), and the results are grouped into terms multiplying $\cos \omega t$, terms multiplying $\sin \omega t$, and higher harmonic terms. The terms multiplying $\sin \omega t$ and the terms multiplying $\cos \omega t$ are then equated to zero, and the higher harmonics are ignored, since they usually contribute little to the solution.

This procedure results in two coupled algebraic equations involving the unknown amplitudes and phases. Applying a similar procedure to equations (5b) to (5d) yields six more equations. The end result is a set of eight nonlinear algebraic equations for the eight unknowns A, B, C, D, ϕ, ψ, χ, and ω. Particular solutions to these equations are now presented.

Two-mode standing-wave solution.- A possible approximate solution to equations (5) is given by

$$a_1(t) = A \cos \omega t$$
$$a_2(t) = B \cos(\omega t + \phi)$$
$$b_1(t) = 0$$
$$b_2(t) = 0$$

(9)

which is the same as equations (8) with C = 0 and D = 0. In this case, the nondimensional shell deflection is given by

$$\frac{w(x,\theta,t)}{h} = \left[A \cos \omega t \sin \frac{\pi x}{L} + B \cos(\omega t + \phi)\sin \frac{2\pi x}{L} \right] \cos n\theta + \frac{\sqrt{\epsilon}}{8} \left\{ A^2 \left[1 + \cos 2\omega t \right] \sin^2 \frac{\pi x}{L} \right.$$

$$\left. + B^2 \left[1 + \cos 2(\omega t + \phi) \right] \sin^2 \frac{2\pi x}{L} + 2AB \left[\cos(2\omega t + \phi) + \cos \phi \right] \sin \frac{\pi x}{L} \sin \frac{2\pi x}{L} \right\} \quad (10)$$

Solutions represented by equations (9) and (10) are referred to as "two-mode standing-wave flutter."

For this type of flutter, the algebraic equations which result from the method of harmonic balance reduce to the following four equations involving A, B, ϕ, and ω.

10

$$\Delta\omega A + \frac{\epsilon}{8} A\left\{\frac{\Delta\omega}{2}\left[\frac{3}{2} A^2 + B^2(2 + \cos 2\phi)\right] - \left[2(k_3 - k_4 - 4k_2) + \omega^2\right]B^2\sin 2\phi\right\}$$

$$- fB \sin \phi\left[1 + \frac{\epsilon}{5}\left(\frac{1}{4} A^2 + \frac{3}{7} B^2\right)\right] + \frac{\epsilon^2}{2} AB^2\left[(l_2 - l_4)A^2 + (l_3 + l_5)B^2\right]\sin 2\phi = 0 \qquad (11a)$$

$$\left(\omega^2 - \omega_{1n}^2\right)A + \frac{\epsilon}{16} A\left\{3\left[4(k_1 - k_2) + \omega^2\right]A^2 + 2\left[2(k_3 - k_4 - 4k_2) + \omega^2\right]B^2(2 + \cos 2\phi)\right.$$

$$\left. + \Delta\omega B^2\sin 2\phi\right\} + fB \cos \phi\left[1 + \frac{3}{5}\epsilon\left(\frac{1}{4} A^2 + \frac{1}{7} B^2\right)\right] - \frac{\epsilon^2}{8} A\left\{7l_1A^4 + B^2\left[2(l_2 - l_4)A^2\right.\right.$$

$$\left.\left. + (l_3 + l_5)B^2\right](3 + 4 \cos 2\phi)\right\} = 0 \qquad (11b)$$

$$\Delta\omega B + \frac{\epsilon}{8} B\left\{\frac{\Delta\omega}{2}\left[A^2(2 + \cos 2\phi) + \frac{3}{2} B^2\right] + \left[2\left(k_3 - k_4 - 4k_2\right) + \omega^2\right]A^2\sin 2\phi\right\}$$

$$- fA \sin \phi\left[1 + \frac{\epsilon}{5}\left(\frac{3}{4} A^2 + \frac{1}{7} B^2\right)\right] - \frac{\epsilon^2}{2} A^2B\left[(l_3 + l_5)B^2 + (l_2 - l_4)A^2\right]\sin 2\phi = 0 \qquad (11c)$$

$$\left(\omega^2 - \omega_{2n}^2\right)B + \frac{\epsilon}{16} B\left\{2\left[2\left(k_3 - k_4 - 4k_2\right) + \omega^2\right]A^2(2 + \cos 2\phi) + 3\left[4\left(k_5 - 16k_2\right) + \omega^2\right]B^2\right.$$

$$\left. - \Delta\omega A^2\sin 2\phi\right\} - fA \cos \phi\left[1 + \frac{3}{5}\epsilon\left(\frac{1}{4} A^2 + \frac{1}{7} B^2\right)\right] - \frac{\epsilon^2}{8} B\left\{7l_6B^4 + A^2\left[2(l_3 + l_5)B^2\right.\right.$$

$$\left.\left. + (l_2 - l_4)A^2\right](3 + 4 \cos 2\phi)\right\} = 0 \qquad (11d)$$

It may be noted that these equations reduce to those already presented in reference 6 when the ϵ^2 terms are neglected. Solutions to equations (11) were obtained by a generalization of Newton's Method. (See appendix C.) A typical calculation is discussed under "Results and Discussion."

The results were found to be sensitive to small amounts of structural damping. The influence of this damping was estimated by assuming viscous damping and modifying the parameter Δ as follows. A new parameter Δ' was introduced in place of Δ, where

$$\Delta' = \Delta + 2\zeta\omega_{1n} \qquad (12)$$

11

In this expression, Δ is the aerodynamic damping and ζ represents the structural modal damping. The new parameter Δ' was introduced into equations (11) in place of Δ, and the limit cycle calculations were repeated for various values of damping ratio ζ.

Under certain conditions, the two-mode limit cycle was found to be unstable with respect to disturbances in the quiescent modes b_1 and b_2. (The procedure used to determine stability of the limit cycles is discussed in a subsequent section of this report.) For some cases, it was found that if the modes b_1 and b_2 were disturbed from zero, their amplitudes increased with time. For nonzero values of b_1 and b_2, all four modes participate in the flutter, and "traveling-wave flutter" usually results. Traveling-wave flutter is discussed in the following section.

Four-mode traveling-wave solution.- A second approximate solution to equations (5) is given by

$$\left. \begin{aligned} a_1(t) &= A \cos \omega t \\ a_2(t) &= B \cos(\omega t + \phi) \\ b_1(t) &= \pm A \sin \omega t \\ b_2(t) &= \pm B \sin(\omega t + \phi) \end{aligned} \right\} \tag{13}$$

which is the same as equations (8) with $A = C$, $B = D$, $\psi = \mp \frac{\pi}{2}$, and $\chi = \phi \mp \frac{\pi}{2}$. The nondimensional shell deflection corresponding to equations (13) can be written as

$$\frac{w(x,\theta,t)}{h} = A \sin \frac{\pi x}{L} \cos(n\theta \mp \omega t) + B \sin \frac{2\pi x}{L} \cos(n\theta \mp \phi \mp \omega t) + \frac{\sqrt{\epsilon}}{4}\left[A^2 \sin^2 \frac{\pi x}{L} + B^2 \sin^2 \frac{2\pi x}{L} \right.$$

$$\left. + 2AB \sin \frac{\pi x}{L} \sin \frac{2\pi x}{L} \cos \phi \right] \tag{14}$$

The first two terms of this expression for w/h represent circumferentially traveling waves. Hence, this type of flutter is referred to as "traveling-wave flutter."

For this type of flutter, the algebraic equations obtained by the method of harmonic balance again reduce to four equations involving A, B, ϕ, and ω as unknowns. These equations are

$$\Delta \omega A - \frac{\epsilon}{2}\left(k_3 - 8k_2\right)AB^2 \sin 2\phi - fB \sin \phi \left[1 - \frac{\epsilon}{5}\left(A^2 - \frac{4}{7}B^2\right)\right] + \frac{\epsilon^2}{2} AB^2\left(l_2 A^2 + l_3 B^2\right)\sin 2\phi = 0 \tag{15a}$$

$$\left(\omega^2 - \omega_{1n}^2\right)A + \frac{\epsilon}{2} A\left\{2\left(k_1 - k_2\right)A^2 + \left[k_3 - 2k_4 + \left(k_3 - 8k_2\right)\cos 2\phi\right]B^2\right\} + fB \cos \phi$$

$$\times \left[1 + \frac{\epsilon}{5}\left(A^2 + \frac{4}{7} B^2\right)\right] - \epsilon^2 A\left[l_1 A^4 - 2l_4 A^2 B^2 + l_5 B^4 + \left(l_2 A^2 + \frac{1}{2} l_3 B^2\right)B^2(1 + \cos 2\phi)\right] = 0$$

(15b)

$$\Delta\omega B + \frac{\epsilon}{2}\left(k_3 - 8k_2\right)A^2 B \sin 2\phi - fA \sin \phi\left[1 + \frac{\epsilon}{5}\left(A^2 - \frac{4}{7} B^2\right)\right] - \frac{\epsilon^2}{2} A^2 B\left(l_2 A^2 + l_3 B^2\right)\sin 2\phi = 0$$

(15c)

$$\left(\omega^2 - \omega_{2n}^2\right)B + \frac{\epsilon}{2} B\left\{2\left(k_5 - 16k_2\right)B^2 + \left[k_3 - 2k_4 + \left(k_3 - 8k_2\right)\cos 2\phi\right]A^2\right\} - fA \cos \phi$$

$$\times \left[1 + \frac{\epsilon}{5}\left(A^2 + \frac{4}{7} B^2\right)\right] - \epsilon^2 B\left[l_6 B^4 + 2l_5 A^2 B^2 - l_4 A^4 + \left(\frac{1}{2} l_2 A^2 + l_3 B^2\right)A^2(1 + \cos 2\phi)\right] = 0$$

(15d)

It is interesting to note that equations (15) are appreciably less complicated than equations (11) for the standing-wave flutter. This condition is mainly due to the fact that for the assumed traveling-wave solution given by equations (13), all the nonlinear terms containing time derivatives in equations (5) cancel out; further discussion of this point is given in a subsequent section of the report.

Equations (15) were also solved by the technique outlined in appendix C; the influence of damping was again estimated by using Δ' in place of Δ (eq. (12)).

In addition to the solutions represented by equations (9) and (13), one other type of limit cycle flutter was observed. This final type of flutter is designated as "four-mode in-phase flutter" and is discussed in the following section.

Four-mode in-phase solution.- Another approximate solution to equations (5) is

$$\left.\begin{array}{l} a_1(t) = A \cos \omega t \\ a_2(t) = B \cos(\omega t + \phi) \\ b_1(t) = \pm A \cos \omega t \\ b_2(t) = \pm B \cos(\omega t + \phi) \end{array}\right\}$$

(16)

which is the same as equations (8) with $A = C$, $B = D$, $\psi = 0,\pi$ and $\chi = \phi + 0,\pi$. The nondimensional shell deflection corresponding to this solution can be expressed as

13

$$\frac{w(x,\theta,t)}{h} = \sqrt{2}\left[A\cos\omega t\sin\frac{\pi x}{L} + B\cos(\omega t + \phi)\sin\frac{2\pi x}{L}\right]\cos\left(n\theta \mp \frac{\pi}{4}\right) + \frac{\sqrt{\epsilon}}{4}\left\{A^2(1 + \cos 2\omega t)\right.$$

$$\times \sin^2\frac{\pi x}{L} + B^2\left[1 + \cos 2(\omega t + \phi)\right]\sin^2\frac{2\pi x}{L} + 2AB\left[\cos(2\omega t + \phi) + \cos\phi\right]\sin\frac{\pi x}{L}\sin\frac{2\pi x}{L}\right\} \quad (17)$$

As may be seen by comparing equation (17) with equation (10), this deflection shape is equivalent to that for two-mode standing-wave flutter. The only difference is that one deflection shape is rotated circumferentially with respect to the other by $\mp\pi/4$ radians. The values of A and B for the two types of flutter are related by the $\sqrt{2}$ factor since $\sin(\pi/4) = \cos(\pi/4) = 1/\sqrt{2}$.

The algebraic equations for four-mode in-phase flutter are also related to those for the two-mode flutter. One set can be transformed into the other by multiplying the amplitudes A and B by the $\sqrt{2}$ factor. Thus, it can be said that four-mode in-phase flutter is simply another form of two-mode standing-wave flutter, and the two cases need not be treated separately.

Although the limit cycle solutions obtained by the method of harmonic balance have been discussed in some detail, several unanswered questions still remain. First of all, there is no guarantee that the three types of limit cycles just described are the only limit cycle solutions to equations (5). Possibly other more general limit cycles exist where ψ is not 0, $\pm\pi/2$ or π, where $A \neq C$, $B \neq D$, and so forth. Secondly, the question of the stability of the various limit cycles has not been investigated. In order to study these questions, equations (5) were integrated numerically on a digital computer.

Solutions by Numerical Integration — Limit Cycle Stability

The method of Runge-Kutta-Gill was used to integrate equations (5) numerically on a digital computer. The procedure used was to begin with a set of initial velocities and displacements for a_1, a_2, b_1, and b_2 and integrate forward in time until either the amplitudes decayed to zero or some sort of steady-state limit cycle was reached.

The stability of the limit cycles was also examined numerically. Once a limit cycle solution was obtained from the algebraic equations (11) or (15), it was possible to determine a set of initial conditions which corresponded to the limit cycle. The numerical integration was then started with these particular initial conditions to verify the existence of the limit cycle. To test its stability, small perturbations were introduced numerically in the initial conditions, and caused them to deviate slightly from those corresponding to the limit cycle. Then equations (5) were integrated forward in time by using these perturbed initial conditions. If the numerical integration resulted in the same limit cycle solution which was originally perturbed, that solution was said to be stable. However, if

14

the numerical integration did not return to the original limit cycle, then the solution was said to be unstable. This procedure was used to determine the stability of the various types of flutter motions discussed previously.

RESULTS AND DISCUSSION

The preceding calculations were carried out for the shell described in references 5 and 6. The shell properties, flow conditions, and loading are as follows:

$$E = 16 \times 10^6 \text{ lb/in}^2 \quad \left(11 \times 10^{10} \text{ N/m}^2\right)$$

$$h = 0.0040 \text{ inch} \quad (0.0001015 \text{ meter})$$

$$L = 15.40 \text{ inches} \quad (0.381 \text{ meter})$$

$$R = 8.00 \text{ inches} \quad (0.203 \text{ meter})$$

$$\rho_s = 0.000833 \text{ lb-sec}^2/\text{in}^4 \quad (8900 \text{ kg/m}^3)$$

$$\nu = 0.350$$

$$M_\infty = 3.00$$

$$a_\infty = 8400 \text{ inches/sec} \quad (213 \text{ m/sec})$$

$$\overline{N}_x = 0$$

$$\overline{N}_\theta = 4 \text{ lb/inch} \quad (701 \text{ n/m})$$

$$p_m = 0.50 \text{ lb/in}^2 \quad (3440 \text{ n/m}^2)$$

The calculations were nondimensionalized by using the two-mode linear results given by equations (C4). Most of these computations were carried out for a circumferential wave number $n = 23$. This value of n was selected since reference 6 shows that it results in the minimum static pressure for flutter according to two-mode linear theory.

Two-Mode Results

The results of the calculations using equations (11) are shown in figures 2 and 3 for the case of no structural damping. Figure 2 is a plot of the variation of the limit cycle amplitudes with the static-pressure parameter f/f_0. Note that for small amplitudes A and B, the curves of figure 2 approach the linear flutter boundary, which occurs at $f/f_0 = 1.0$.
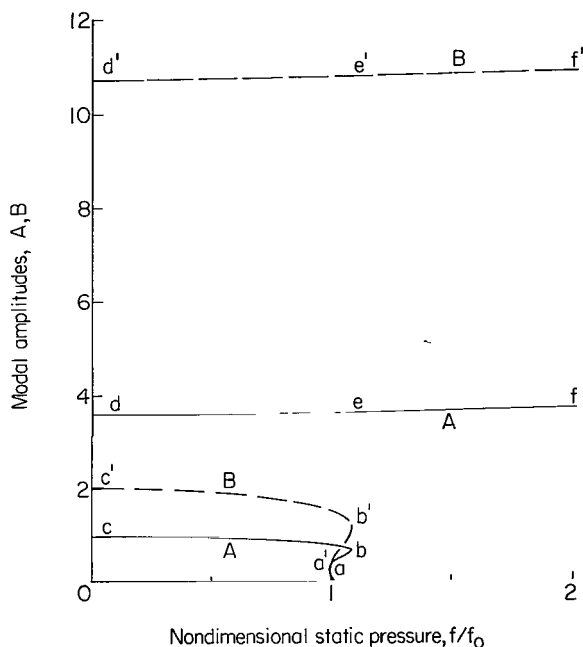
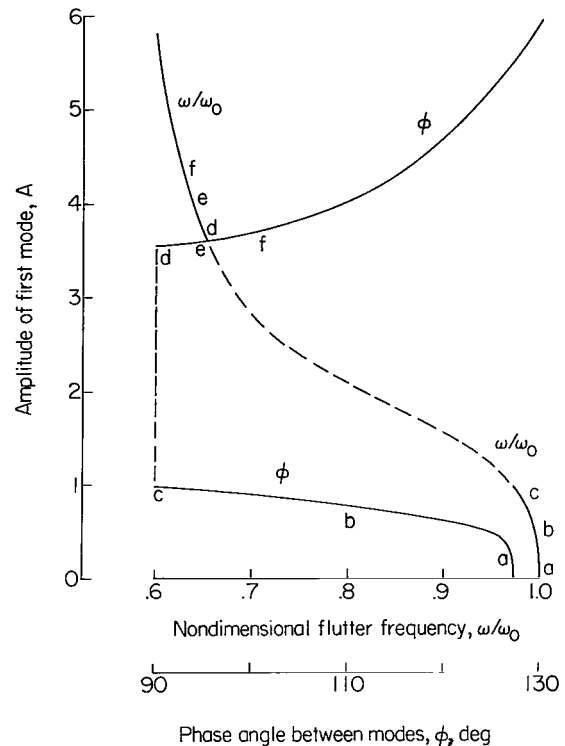Figure 2.- Limit cycle amplitudes. Two-mode flutter.
n = 23; ζ = 0.

Figure 3.- Flutter frequency and phase angle dependence on amplitude. Two-mode flutter. Dashed portions of curves do not represent real solutions but merely serve to indicate the connection between the two branches. n = 23; ζ = 0.

In order to interpret figure 2, imagine a shell flutter experiment and consider what might happen at various values of static pressure, that is, f/f_0. First, consider $f/f_0 < 1$, that is, conditions below the linear flutter boundary, and imagine that the modes $a_1(t)$ and $a_2(t)$ are disturbed from rest. If the disturbances are infinitesimal, they will be damped in time and the shell will not flutter. This result is identical with linear flutter theory.

On the other hand, if the disturbances are of the proper magnitude, limit cycle flutter might occur along segments bc (b'c') or de (d'e') of the curves in figure 2. For example, imagine that $f/f_0 = 0.4$ and the modes are disturbed such that $a_1(t) \approx 1.0$ and $a_2(t) \approx 2.0$. Under these conditions, the shell might experience limit cycle flutter at a point on the bc (b'c') portion of the curves in figure 2. However, numerical stability studies have shown that segments bc (b'c') represent unstable limit cycles; thus, if this limit cycle flutter were disturbed ever so slightly, the amplitudes of a_1 and a_2 would either (a) damp down to zero or (b) increase up to the segments de (d'e') in figure 2. Segments de (d'e') represent stable limit cycle flutter, and further disturbances in a_1 and a_2 would just result in a return to the limit cycle, that is, to flutter with $A \approx 3.6$ and $B \approx 10.7$.

16

Now consider what might happen above the linear flutter boundary, that is, at $f/f_0 > 1.0$. Under these conditions, infinitesimal disturbances in the modes a_1 and a_2 increase with time. Linear theory indicates that the flutter amplitudes increase without bound; however, with nonlinearities present, the amplitudes eventually stabilize at points along ab (a'b') or ef (e'f') of the curves in figure 2. The branch that will be reached (ab or ef) depends upon the initial disturbances as well as f/f_0.

It is of interest to note that the lower branches (abc, a'b'c') of the curves shown in figure 2 are practically identical with the results given in figure 9 of reference 6. However, since terms of order ϵ^2 have been retained in the present analysis but were neglected in reference 6, the present results have additional branches (def, d'e'f') running off to the right with increasing aerodynamic pressure.

In order to define two-mode limit cycle flutter fully, it is necessary to specify the flutter frequency and phase angle in addition to the modal amplitudes A and B. Figure 3 gives the flutter frequency ω/ω_0 and phase angle ϕ for various values of the modal amplitude A. The curves of figure 3 have been labeled to correspond with branches abc and def of figure 2. Note that the dashed portions of the curves in figure 3 do not represent real solutions; they merely serve to indicate the connection between the two branches. The flutter frequency is seen to decrease continuously with increasing flutter amplitude, whereas the phase angle first decreases to 90° and then increases at the higher amplitudes. Decreasing frequency with amplitude is characteristic of the "softening" type of nonlinearity noted in the vibrations of cylindrical shells. (See ref. 8.)

Figure 4 shows sample time traces of the steady-state motion obtained from the numerical integration of equations (5) at $f/f_0 = 2.0$. To obtain these results, the modal amplitudes b_1 and b_2 were set equal to zero in the numerical integration. For this particular case, the steady-state motion contains a small amount of beating. The influence of the nonlinearities is exhibited by the distinctly nonsinusoidal character of the a_1 curve in figure 4. Despite this nonsinusoidal behavior, the average modal amplitudes, the predominant frequency, and the phase angle between the modes obtained from the curves of figure 4 agree well with those predicted by the harmonic balance method. (See fig. 2, for example.)

The influence of structural damping on the two-mode results is shown in figure 5. For $\zeta = 0$ (zero damping), the theory indicates that the limit cycle curves extend to the left until $f = 0$. With damping present, however, the results are fundamentally different. The amplitude curves now do not continue to the left until $f = 0$, but instead bend up steeply at small values of f. One would expect that they would then bend again and approach the upper branches (def, d'e'f') for increasing f. The second-mode amplitude B does indeed behave in this way. However, the first-mode amplitude A actually overshoots and then approaches the branch def from above. As a consequence, the curves
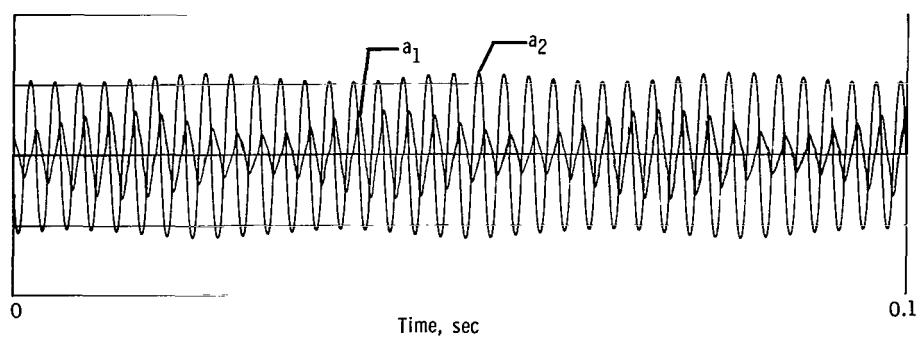
Figure 4.- Numerical integration results. Two-mode flutter; $f/f_0 = 2.0$. $n = 23$; $\zeta = 0$.
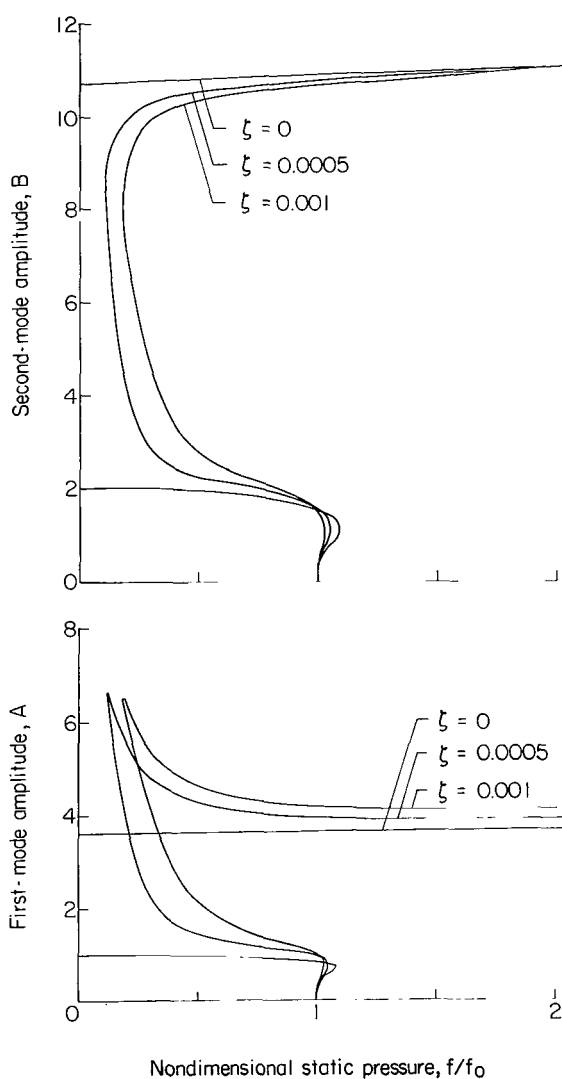

Figure 5.- Two-mode results, with damping. $n = 23$.

for A exhibit horizontal tangencies at $f/f_O = 1.42$ and 1.46 for $\zeta = 0.0005$ and 0.001, respectively.

Numerical stability studies indicated that the damped curves of figure 5 were unstable to the left of the horizontal tangencies just mentioned. For example, with $\zeta = 0.001$, numerical integration of equations (5) was carried out for $f/f_O = 0.38$ and 1.20 in an attempt to obtain limit cycles at these points. Initial conditions for the numerical integration were obtained from the curves of figure 5. In both cases, the amplitudes decayed to zero and no limit cycle was obtained. On the other hand, when a similar procedure was tried at $f/f_O = 1.60$, a steady-state limit cycle resulted. These results show that the damped two-mode limit cycle solutions have a stability boundary (in terms of f/f_O) between 1.2 and 1.6. It is suspected that the boundary occurs at the point of horizontal tangency ($f/f_O = 1.46$). The boundary location is difficult to pinpoint exactly by using numerical integration, since near-zero damping and long integration times are involved.

These stability studies thus identified segments of the damped curves in figure 5 (to the right of $f/f_O = 1.42$ and 1.46) which represent limit cycles which are stable with respect to disturbances in the modes a_1 and a_2. When other disturbances were considered, however, it was found that the two-mode limit cycles were unstable with respect to the modes b_1 and b_2. This instability with respect to the b-modes usually leads to traveling-wave flutter.

Traveling-Wave Results

Results for traveling-wave flutter were calculated from equations (15) and are shown in figures 6 to 8. Figure 6 shows the variation of modal amplitude with aerodynamic-pressure curves. These curves are fundamentally different from the corresponding ones for standing-wave flutter in that they first proceed upward with negative slope until a vertical tangency occurs at a finite value of the aerodynamic pressure. The curves then bend back to positive slope and proceed indefinitely to the right, the first-mode amplitude being larger than the second, that is, $A > B$. Note that B was larger than A for the standing-wave flutter at large amplitudes.

Figure 7 shows how the flutter frequency and phase angle between the modes vary with the traveling-wave flutter amplitude. In this case, the flutter frequency first decreases very slightly and then increases with amplitude. This result is in contrast to the standing-wave flutter, where the frequency decreased with increasing amplitude. Note that the amount of frequency shift is very much smaller here than for the standing-wave case. The large softening nonlinearity exhibited by the standing-wave flutter may be attributed to the nonlinear terms involving time derivatives in equations (5). As noted previously, these terms cancel out for the traveling-wave solution, nonlinearities being
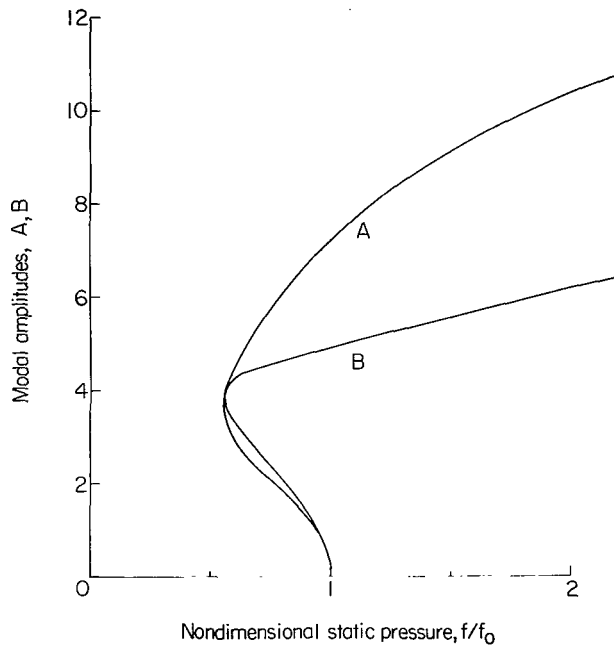
Figure 6.- Limit cycle amplitudes. Traveling-wave flutter.
n = 23; ζ = 0.

Figure 7.- Flutter frequency and phase angle dependence on amplitude. Traveling-wave flutter. n = 23; ζ = 0.

left only in the spring and aerodynamic terms. The final hardening nonlinearity shown by the frequency curve in figure 7 results from the ϵ^2 spring terms in equations (5). The phase angle between modes shown in figure 7 is seen to decrease at high amplitudes, but it does not approach 90° as did the phase for the standing-wave flutter.

The influence of structural damping on the limit cycles for traveling-wave flutter is shown in figure 8. For clarity, only the first-mode amplitude is plotted, since the effect on the second-mode amplitude was very similar. It is seen that the damping shifts the point of vertical tangency slightly to the right, but does not alter the nature of the curves. This result is in contrast to the standing-wave case where a small amount of structural damping caused a large change in the shape of the limit cycle curves.
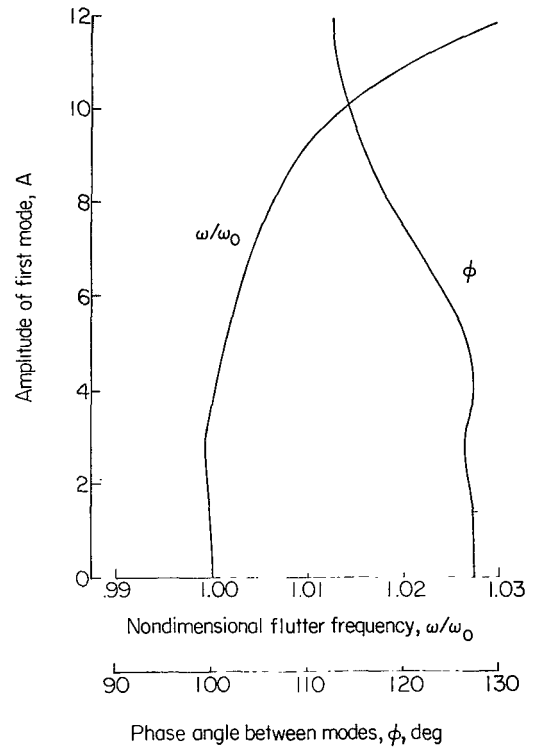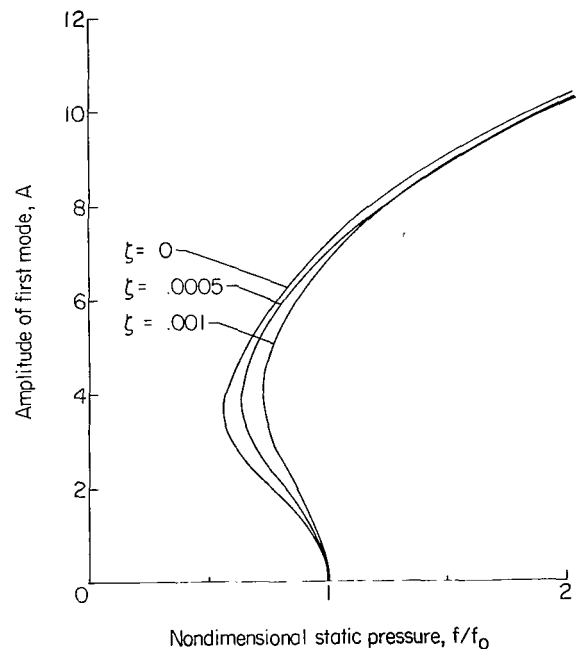
Figure 8.- Influence of damping on the traveling-wave results. n = 23.

20

The results of a numerical integration involving all four modes are shown in figure 9 for $f/f_0 = 2.0$. The initial conditions for this calculation were taken from the limit cycle results of figures 6 and 7. In contrast with standing-wave flutter, these time traces are remarkably close to pure sinusoidal waves of constant amplitude and frequency. The numerical integration results thus verify the amplitudes, frequency, and phase angle predicted for this case by the method of harmonic balance.
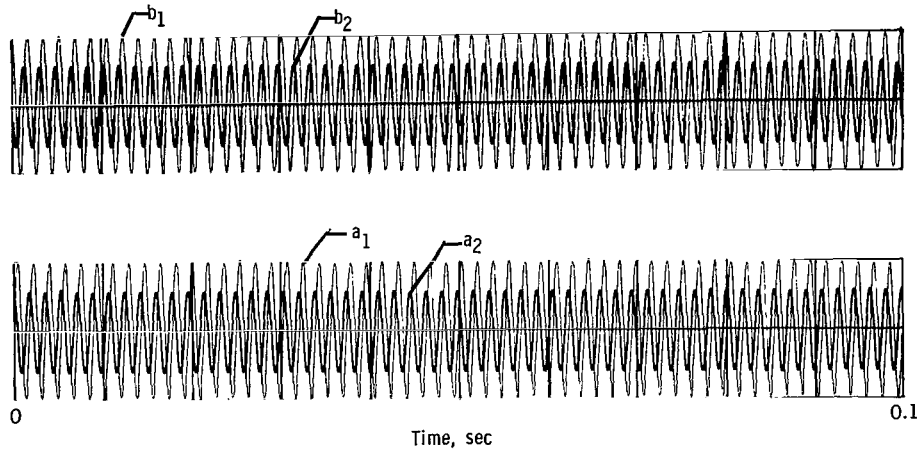

Figure 9.- Numerical integration results. Traveling-wave flutter; $f/f_0 = 2.0$. $n = 23$; $\zeta = 0$.

Stability studies involving perturbations in all four modes showed that only those portions of the curves in figure 6 with positive slope represent stable limit cycle oscillations. The same results would be expected to hold for the cases with structural damping (fig. 8).

Although most of the calculations were made for the $n = 23$ mode(s), qualitatively similar results were obtained for other values of the circumferential wave number n. This fact was demonstrated in reference 6 for two-mode flutter, and it is illustrated in figure 10 for traveling-wave flutter. The curves of figure 10 were calculated for values of n ranging from 17 to 27 and for zero structural damping. Figure 10 shows that the flutter mode depends upon the spatial distribution of the initial disturbances as well as upon their magnitude. For example, at $f = 1.0 \times 10^5$, it is possible to excite limit cycle flutter for various n-values, depending upon the circumferential wave number corresponding to the initial disturbance. If the only disturbances present are infinitesimal, figure 10 shows that the shell will not flutter until $f = 1.405 \times 10^5$, which is the linear flutter boundary for the $n = 23$ mode. Note that regardless of the n-value excited, the minimum limiting amplitudes of flutter given in figure 10 are about 4 to 5 shell

21

thicknesses. This analytical result can be compared with the experimentally observed values of 1 to 2 shell thicknesses reported in reference 5.
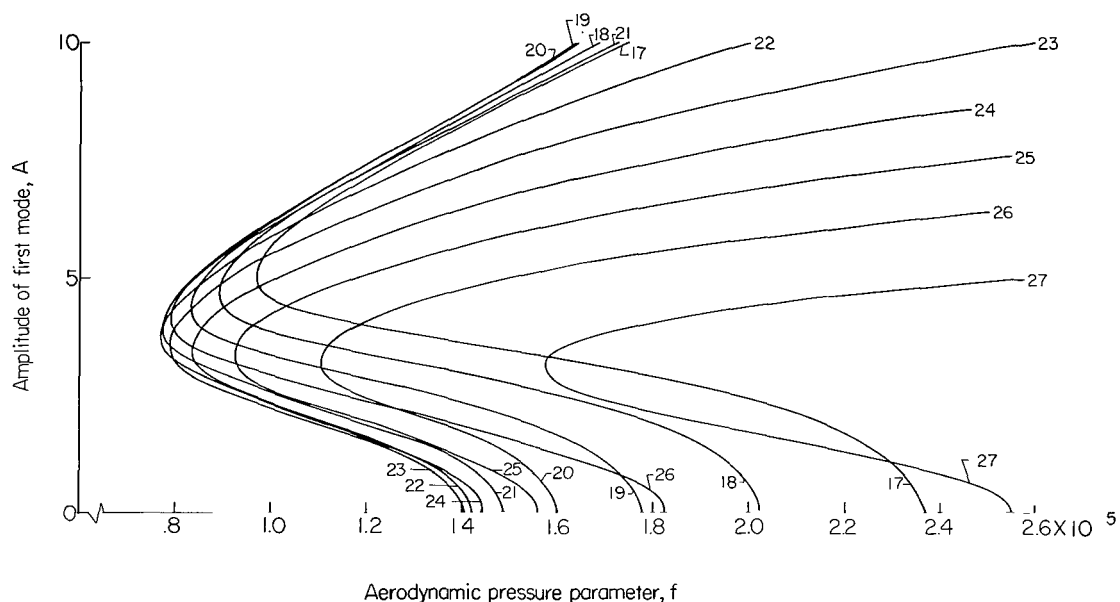

Figure 10.- Limit cycle amplitudes for various values of n. Traveling-wave flutter. $\zeta = 0$.

Once limit cycle flutter is initiated for some value of the circumferential wave number, it is not clear whether modes with other n-values will begin to participate in the motion or not. The experimental results (refs. 4 and 5) suggest that flutter occurs with only single values of n. However, the flutter mode (that is, the value of n) may change as the static pressure is varied. For example, figure 8 of reference 5 shows that the experimental flutter amplitudes do not increase monotonically with increasing stagnation pressure; instead, they exhibit noticeable fluctuations. With respect to figure 10, these experimental results suggest the possibility that the shell might flutter in one mode (n = 22, for example) and then change to another mode (perhaps, n = 23) as the parameter f increases. Such a change in mode might be associated with a jump downward in amplitude from the n = 22 curve to the n = 23 curve in figure 10. Additional mode changes might occur as f is further increased; however, a thorough discussion of this problem would necessitate an analytical study involving combinations of circumferential harmonics n.

CONCLUDING REMARKS

A four-mode nonlinear analysis of cylindrical shell flutter using piston theory and the nonlinear shallow-shell equations has been presented. The results obtained from this analysis lead to the following conclusions:

22

1. The occurrence of circumferentially traveling-wave flutter, which has been observed experimentally, is predictable by the nonlinear theory.

2. Limit cycle flutter in a circumferentially traveling-wave mode can occur below the stability boundary predicted by linear theory. This fact may help to explain the differences between experimental results and linear theory.

3. The two-mode standing-wave limit cycle results were found to be very sensitive to small amounts of structural damping, whereas the traveling-wave results were not.

4. The limit cycle amplitudes predicted by the present analysis are somewhat larger than the experimental results. It is expected that the theoretical limiting amplitudes would be reduced if the longitudinal displacement u was made to vanish at the ends of the shell. Such an axial restraint would be more representative of the experiments than are the boundary conditions satisfied in the present analysis.

5. One limitation of the present study is the fact that it has been restricted to only four modes. It is expected that adding more modes in the axial direction would alter the present results quantitatively but not qualitatively. On the other hand, it is harder to estimate the influence of adding more circumferential modes to the analysis. When the aerodynamic pressure exceeds the linear flutter boundaries of two or more modes with different values of circumferential wave number n, it is not clear how the modes might combine. The answer to this question is left to a future investigation.

Langley Research Center,
        National Aeronautics and Space Administration,
                Langley Station, Hampton, Va., October 31, 1967,
                        124-08-05-08-23.

PARTICULAR SOLUTION TO EQUATION (2)

Define $\alpha = \pi/L$ and $\beta = n/R$. Then a particular solution to equation (2) which corresponds with the assumed deflection shape w is

$$
\begin{aligned}
\frac{F(x,\theta,t)}{Eh} = {} & \frac{\alpha^2}{R(\alpha^2+\beta^2)^2}(A_1\cos n\theta + B_1\sin n\theta)\sin\alpha x + \frac{4\alpha^2}{R(4\alpha^2+\beta^2)^2}(A_2\cos n\theta + B_2\sin n\theta)\sin 2\alpha x - \frac{\alpha^2}{16\beta^2}\left[\frac{1}{2}\left(A_1{}^2 - B_1{}^2\right) + 2\left(A_2{}^2 - B_2{}^2\right)\right]\cos 2n\theta \\[2mm]
& - \frac{\alpha^2}{16\beta^2}\left(A_1B_1 + 4A_2B_2\right)\sin n\theta - \frac{9\alpha^2\beta^2}{4\left(\alpha^2+4\beta^2\right)^2}\left[\left(A_1A_2 - B_1B_2\right)\cos 2n\theta + \left(A_1B_2 + A_2B_1\right)\sin 2n\theta\right]\cos\alpha x \\[2mm]
& + \frac{\alpha^2\beta^2}{4\left(\alpha^2+4\beta^2\right)^2}\left[\left(A_1A_2 - B_1B_2\right)\cos 2n\theta + (A_1B_2 + A_2B_1)\sin 2n\theta\right]\cos 3\alpha x + \frac{\alpha^2\beta^4 R}{2}\left\{-\frac{\sin\alpha x}{\left(\alpha^2+\beta^2\right)^2}\left[\frac{A_1}{2}\left(A_1{}^2 + B_1{}^2\right) + \frac{5A_2}{2}\left(A_1A_2 + B_1B_2\right)\right]\right. \\[2mm]
& - \frac{\sin 2\alpha x}{\left(4\alpha^2+\beta^2\right)^2}\left[2A_2\left(A_2{}^2 + B_2{}^2\right) + \frac{5A_1}{2}\left(A_1A_2 + B_1B_2\right)\right] + \frac{\sin 3\alpha x}{\left(9\alpha^2+\beta^2\right)^2}\left[\frac{A_1}{2}\left(A_1{}^2 + B_1{}^2\right) - 2A_1\left(A_2{}^2 + B_2{}^2\right) - \frac{A_2}{4}\left(A_1A_2 + B_1B_2\right)\right] \\[2mm]
& + \frac{\sin 4\alpha x}{\left(16\alpha^2+\beta^2\right)^2}\left[\frac{A_2}{2}\left(A_1{}^2 + B_1{}^2\right) + \frac{9}{4}A_1(A_1A_2 + B_1B_2)\right] + \frac{\sin 5\alpha x}{\left(25\alpha^2+\beta^2\right)^2}\left[2A_1\left(A_2{}^2 + B_2{}^2\right) + \frac{9}{4}A_2(A_1A_2 + B_1B_2)\right] \\[2mm]
& \left. + \frac{\sin 6\alpha x}{\left(36\alpha^2+\beta^2\right)^2}\left[2A_2\left(A_2{}^2 + B_2{}^2\right)\right]\right\}\cos n\theta + \frac{\alpha^2\beta^4 R}{2}\left\{-\frac{\sin\alpha x}{\left(\alpha^2+\beta^2\right)^2}\left[\frac{B_1}{2}\left(A_1{}^2 + B_1{}^2\right) + \frac{5B_2}{2}(A_1A_2 + B_1B_2)\right]\right. \\[2mm]
& - \frac{\sin 2\alpha x}{\left(4\alpha^2+\beta^2\right)^2}\left[2B_2\left(A_2{}^2 + B_2{}^2\right) + \frac{5B_1}{2}\left(A_1A_2 + B_1B_2\right)\right] + \frac{\sin 3\alpha x}{\left(9\alpha^2+\beta^2\right)^2}\left[\frac{B_1}{2}\left(A_1{}^2 + B_1{}^2\right) - 2B_1\left(A_2{}^2 + B_2{}^2\right) - \frac{B_2}{4}\left(A_1A_2 + B_1B_2\right)\right] \\[2mm]
& \left. + \frac{\sin 4\alpha x}{\left(16\alpha^2+\beta^2\right)^2}\left[\frac{B_2}{2}\left(A_1{}^2 + B_1{}^2\right) + \frac{9B_1}{4}\left(A_1A_2 + B_1B_2\right)\right] + \frac{\sin 5\alpha x}{\left(25\alpha^2+\beta^2\right)^2}\left[2B_1\left(A_2{}^2 + B_2{}^2\right) + \frac{9B_2}{4}(A_1A_2 + B_1B_2)\right] + \frac{\sin 6\alpha x}{\left(36\alpha^2+\beta^2\right)^2}\left[2B_2\left(A_2{}^2 + B_2{}^2\right)\right]\right\}\sin n\theta
\end{aligned}
$$

where A_1, A_2, B_1, and B_2 are functions of time.

APPENDIX B

DEFINITION OF CONSTANTS USED IN EQUATIONS (5)

The linear undamped modal frequencies are given by

$$\omega_{mn}^2 = \frac{1}{\rho_s h}\left\{ D_s\left[\left(\frac{m\pi}{L}\right)^2 + \left(\frac{n}{R}\right)^2\right]^2 + \frac{Eh}{R^2}\frac{(m\pi/L)^4}{\left[(m\pi/L)^2 + (n/R)^2\right]^2} + \left(\frac{m\pi}{L}\right)^2 \overline{N}_x + \left(\frac{n}{R}\right)^2 \overline{N}_\theta \right\}$$

$$(m = 1,2) \qquad (B1)$$

Let $\sigma = \dfrac{\pi/L}{n/R}$; then the coefficients k_1 to k_5 are defined by

$$k_1 = \frac{E\sigma^4}{\rho_s R^2}\left[\frac{1}{\left(\sigma^2 + 1\right)^2} - \frac{\epsilon}{12\left(1 - \nu^2\right)}\right] - \frac{\overline{N}_x}{4\rho_s h}\left(\frac{\pi}{L}\right)^2 \qquad (B2)$$

$$k_2 = \frac{E\sigma^4}{16\rho_s R^2} \qquad (B3)$$

$$k_3 = \frac{E\sigma^4}{\rho_s R^2}\left[\frac{5}{2\left(\sigma^2 + 1\right)^2} + \frac{10}{\left(4\sigma^2 + 1\right)^2} - \frac{41\epsilon}{48\left(1 - \nu^2\right)}\right] - \frac{5\overline{N}_x}{4\rho_s h}\left(\frac{\pi}{L}\right)^2 \qquad (B4)$$

$$k_4 = \frac{\sigma}{16\rho_s R^2}\left[\frac{81}{\left(\sigma^2 + 4\right)^2} + \frac{1}{\left(9\sigma^2 + 4\right)^2}\right] \qquad (B5)$$

$$k_5 = \frac{16E\sigma}{\rho_s R^2}\left[\frac{1}{\left(4\sigma^2 + 1\right)^2} - \frac{\epsilon}{12\left(1 - \nu^2\right)}\right] - \frac{\overline{N}_x}{\rho_s h}\left(\frac{\pi}{L}\right)^2 \qquad (B6)$$

Similarly, the coefficients l_1 to l_6 are given by

$$l_1 = \frac{3}{16}\frac{E\sigma^4}{\rho_s R^2}\left[\frac{1}{\left(\sigma^2 + 1\right)^2} + \frac{1}{\left(9\sigma^2 + 1\right)^2}\right] \qquad (B7)$$

$$l_2 = \frac{E\sigma^4}{8\rho_S R^2}\left[\frac{5}{\left(\sigma^2+1\right)^2} + \frac{25}{2\left(4\sigma^2+1\right)^2} - \frac{1}{2\left(9\sigma^2+1\right)^2} + \frac{117}{8\left(16\sigma^2+1\right)^2}\right] \tag{B8}$$

$$l_3 = \frac{E\sigma^4}{2\dot\rho_S R^2}\left[\frac{25}{8\left(\sigma^2+1\right)^2} + \frac{5}{\left(4\sigma^2+1\right)^2} + \frac{17}{32\left(9\sigma^2+1\right)^2} + \frac{225}{32\left(25\sigma^2+1\right)^2}\right] \tag{B9}$$

$$l_4 = \frac{E\sigma^4}{2\rho_S R^2}\left[\frac{1}{\left(9\sigma^2+1\right)^2} - \frac{1}{8\left(16\sigma^2+1\right)^2}\right] \tag{B10}$$

$$l_5 = \frac{E\sigma^4}{\rho_S R^2}\left[\frac{1}{\left(9\sigma^2+1\right)^2} + \frac{1}{\left(25\sigma^2+1\right)^2}\right] \tag{B11}$$

$$l_6 = \frac{3E\sigma^4}{\rho_S R^2}\left[\frac{1}{\left(4\sigma^2+1\right)^2} + \frac{1}{\left(36\sigma^2+1\right)^2}\right] \tag{B12}$$

APPENDIX C

SOLUTION OF THE ALGEBRAIC EQUATIONS

The complexity of the algebraic equations (11) and (15) precludes the possibility of a closed-form solution, and a numerical method must be employed. Such a method was introduced in reference 12 and yielded satisfactory results. The method as used herein is outlined in the following paragraphs.

The four unknowns A, B, ϕ, and ω in equations (11) and (15) are required as functions of the aerodynamic pressure p_∞ for a given shell geometry, speed of sound, and Mach number of the airstream, and for various values of the circumferential wave number n. The aerodynamic pressure comes into the algebraic equations through the two parameters Δ and f. The damping parameter Δ' (see eq. (12)) may be put in the form:

$$\Delta' = \Delta + 2\zeta\omega_{1n} = \kappa f + 2\zeta\omega_{1n} \tag{C1}$$

where $\kappa = 3L/8M_\infty a_\infty$. Hence, the parameter f may be used to represent the aerodynamic pressure.

It is convenient for the calculations required herein to treat A as known and B, ω, f, and ϕ as unknowns. Let the four component vector x_i (i = 1 to 4) denote the unknowns such that $x_1 = B$, $x_2 = \omega$, $x_3 = f$, and $x_4 = \phi$; then each set of equations (11) or (15) is of the functional form

$$K_j(x_i) = 0 \qquad\qquad (i,j = 1,2,3,4) \tag{C2}$$

The solutions to these equations are obtained by a generalization of Newton's method to many variables as follows. If x_{io} is a good initial approximation to the sought-for solution x_i such that $x_{io} = x_i - \delta x_i$, then by expanding equations (B2) in a Taylor series from x_{io} to x_i,

$$K_j(x_{io}) + \sum_{l=1}^{4} \left.\frac{\partial K_j}{\partial x_l}\right|_{x_i=x_{io}} \delta x_l \approx 0 \tag{C3}$$

Now the δx_i may be found from equation (C3), since by definition $K_j(x_{io}) \neq 0$. When this is done, the new approximation for x_i is $x_{i1} = x_{io} + \delta x_i$, and the foregoing procedure is repeated over again until the corrections δx_i become negligibly small.

APPENDIX C

The initial approximation used to start this process is that obtained from the linear flutter problem. This approximation results from the linearization of equations (11) or (15) and may be shown to be

$$
\left.
\begin{aligned}
A &= B \\[2mm]
\omega^2 &= \omega_0^2 = \frac{\omega_{1n}^2 + \omega_{2n}^2}{2} \\[2mm]
f = f_0 &= \frac{2\zeta\omega_{1n}\kappa\omega_0^2 + \sqrt{\left(1 - \kappa^2\omega_0^2\right)\left(\omega_0^2 - \omega_{1n}^2\right)^2 + \left(2\zeta\omega_{1n}\omega_0\right)^2}}{1 - \kappa^2\omega_0^2} \\[2mm]
\phi = \phi_0 &= \pi - \tan^{-1}\left[\frac{\left(\kappa f_0 + 2\zeta\omega_{1n}\right)\omega_0}{\omega_0^2 - \omega_{1n}^2}\right]
\end{aligned}
\right\}
\qquad (C4)
$$

Initially, A is taken to be a small number, and the linear solution given in equation (C3) is used to start the iteration process. Thereafter, A is increased by a small amount, and the solution for the previous value of A is used to restart the iterations.

28

REFERENCES

1. Fung, Y. C. B.: A Summary of the Theories and Experiments on Panel Flutter. AFOSR TN 60-224, U.S. Air Force, May 1960.

2. Fung, Y. C.: Some Recent Contributions to Panel Flutter Research. AIAA J., vol. 1, no. 4, Apr. 1963, pp. 898-909.

3. Johns, D. J.: A Survey on Panel Flutter. AGARD Advisory Rept. 1, Nov. 1965.

4. Stearman, R. O.; Lock, M. H.; and Fung, Y. C.: Ames Tests on the Flutter of Cylindrical Shells. SM 62-37, Graduate Aeron. Labs., California Inst. Technol., Dec. 1962.

5. Olson, Mervyn D.; and Fung, Y. C.: Supersonic Flutter of Circular Cylindrical Shells Subjected to Internal Pressure and Axial Compression. AIAA J., vol. 4, no. 5, May 1966, pp. 858-864.

6. Olson, Mervyn D.; and Fung, Y. C.: Comparing Theory and Experiment for the Supersonic Flutter of Circular Cylindrical Shells. AIAA J., vol. 5, no. 10, Oct. 1967, pp. 1849-1856.

7. Chu, Hu-Nan: Influence of Large Amplitudes on Flexural Vibrations of a Thin Circular Cylindrical Shell. J. Aerospace Sci., vol. 28, no. 8, Aug. 1961, pp. 602-609.

8. Evensen, David A.: Nonlinear Flexural Vibrations of Thin-Walled Circular Cylinders. NASA TN D-4090, 1967.

9. Evensen, David A.: A Theoretical and Experimental Study of the Nonlinear Flexural Vibrations of Thin Circular Rings. NASA TR R-227, 1965.

10. Minorsky, Nicholas: Nonlinear Oscillations. D. Van Nostrand Co., Inc., c.1962.

11. Cunningham, W. J.: Introduction to Nonlinear Analysis. McGraw-Hill Book Co., Inc., c.1958.

12. Olson, Mervyn D.: On Comparing Theory and Experiment for the Supersonic Flutter of Circular Cylindrical Shells. AFOSR 66-0944, U.S. Air Force, June 1966.

"The aeronautical and space activities of the United States shall be conducted so as to contribute . . . to the expansion of human knowledge of phenomena in the atmosphere and space. The Administration shall provide for the widest practicable and appropriate dissemination of information concerning its activities and the results thereof."

—NATIONAL AERONAUTICS AND SPACE ACT OF 1958

NASA SCIENTIFIC AND TECHNICAL PUBLICATIONS

TECHNICAL REPORTS: Scientific and technical information considered important, complete, and a lasting contribution to existing knowledge.

TECHNICAL NOTES: Information less broad in scope but nevertheless of importance as a contribution to existing knowledge.

TECHNICAL MEMORANDUMS: Information receiving limited distribution because of preliminary data, security classification, or other reasons.

CONTRACTOR REPORTS: Scientific and technical information generated under a NASA contract or grant and considered an important contribution to existing knowledge.

TECHNICAL TRANSLATIONS: Information published in a foreign language considered to merit NASA distribution in English.

SPECIAL PUBLICATIONS: Information derived from or of value to NASA activities. Publications include conference proceedings, monographs, data compilations, handbooks, sourcebooks, and special bibliographies.

TECHNOLOGY UTILIZATION PUBLICATIONS: Information on technology used by NASA that may be of particular interest in commercial and other non-aerospace applications. Publications include Tech Briefs, Technology Utilization Reports and Notes, and Technology Surveys.

Details on the availability of these publications may be obtained from:

SCIENTIFIC AND TECHNICAL INFORMATION DIVISION

NATIONAL AERONAUTICS AND SPACE ADMINISTRATION

Washington, D.C. 20546